
Article:
Zilinskaite, S., Reeves-McLaren, N. and Boston, R. (2022) Xanthan gum as a water-based binder for P3-Na2/3Ni1/3Mn2/3O2. Frontiers in Energy Research, 10. 909486.

https://doi.org/10.3389/fenrg.2022.909486

---

frontiers | Frontiers in Energy Research

TYPE Original Research
PUBLISHED 23 August 2022
DOI 10.3389/fenrg.2022.909486

OPEN ACCESS

EDITED BY
Nuria Tapia-Ruiz,
Lancaster University, United Kingdom

REVIEWED BY
Hari Raj,
École Nationale Supérieure d'ingénieurs De Caen, France
Baofeng Wang,
Shanghai University of Electric Power, China
Mauro Francesco Sgroi,
Centro Ricerche FIAT, Italy

*CORRESPONDENCE
Rebecca Boston,
r.boston@sheffield.ac.uk

SPECIALTY SECTION
This article was submitted to Electrochemical Energy Conversion and Storage, a section of the journal Frontiers in Energy Research

RECEIVED 31 March 2022
ACCEPTED 27 July 2022
PUBLISHED 23 August 2022

CITATION
Zilinskaite S, Reeves-McLaren N and Boston R (2022), Xanthan gum as a water-based binder for P3-$Na_{2/3}Ni_{1/3}Mn_{2/3}O_2$.
Front. Energy Res. 10:909486.
doi: 10.3389/fenrg.2022.909486

Xanthan gum as a water-based binder for P3-$Na_{2/3}Ni_{1/3}Mn_{2/3}O_2$

Silvija Zilinskaite, Nik Reeves-McLaren and Rebecca Boston*

Department of Materials Science and Engineering, University of Sheffield, Sheffield, United Kingdom

P3-$Na_{2/3}Ni_{1/3}Mn_{2/3}O_2$ (P3-NNM) is a promising cathode material for Na-ion batteries, although large volume expansions during cycling mean that challenges around suitable binders still remain. This study reports the use of xanthan gum as a water-soluble, easy to handle, and sustainable biopolymer binder in conjunction with a P3-$Na_{2/3}Ni_{1/3}Mn_{2/3}O_2$-positive electrode material. The conditions for recovering pristine P3-NNM powders, following water-based processing, are established, and the electrochemical performance of cells prepared using the xanthan gum binder are compared to the more traditional polyvinylidene fluoride. Comparable discharge capacities are observed regardless of the binder choice, at *ca.* 115 mA h g^{-1} (77 mAh g^{-1} after 50 cycles; 0.1 C between 2.0 and 4.2 V). The xanthan gum binder cells also show a similar rate capability and slightly higher capacities at faster c-rates *vs.* polyvinylidene fluoride, making xanthan gum a viable alternative to the traditional organic binders for water-stable cathode materials.

KEYWORDS

xanthan gum, water-based binder, sodium ion battery, cathode, electrochemistry

Introduction

Current work on Na-ion batteries often focuses on understanding and enhancing the properties of promising cathode and anode materials. When these are critical steps on the route to commercialization, development of novel battery technologies also provides the opportunity to investigate and implement more sustainable chemicals and electrode fabrication processes across the broader remit of the cell assembly. Binders, for example, play a key role in the stability and architecture of electrode materials. However, binders are not often the central focus for development.

Polyvinylidene fluoride (PVDF) is a commonly used binder in both Li- and Na-ion batteries due to its electrochemical and thermal stability, and good adhesion between the current collector and electrode (R.-R. Li et al., 2021a; Lingappan et al., 2021). During cell fabrication, N-methyl pyrrolidone (NMP) is usually used as a solvent for PVDF. NMP is costly and toxic, and PVDF can be difficult to recycle (Versaci et al., 2017; Patra et al., 2018), making this combination a poor choice for low-cost sustainable batteries from preparation to recycling. In addition, PVDF may not be an appropriate binder for sodium ion batteries as it can only accommodate volume changes of 10–15%. If exceeded, the active particles can become disconnected from the matrix and no longer contribute to capacity (Chen et al., 2003; Lingappan et al., 2021). Due to the larger size of the Na ion (*vs.* Li), many Na-ion materials exhibit a high degree of volume change during cycling (Guerfi

et al., 2007). This has been shown to impact the performance in, for example, Si anodes (S. Li et al., 2021b; Lingappan et al., 2021; Zhao et al., 2021), as the large volume changes can lead to mechanical failure. Na-layered transition metal oxides can also exhibit up to 20% volume change, for example, during the P2-O2 transition upon Na deintercalation in P2-$Na_{2/3}Ni_{1/3}Mn_{2/3}O_2$ (Yabuuchi et al., 2014; Liu et al., 2021), so PVDF may not be the optimal binder for these materials. P3-type Na materials are promising candidates for Na-ion cathodes (J. Liu et al., 2020a; Shi et al., 2021; Song et al., 2019). However, they exhibit even larger volume changes and distortions than P2-type materials (Guo et al., 2016; Zhang, 2019). Binder choice, taking into account the different requirements of these emergent cathode materials, is therefore the key to ensuring cell stability and presents an opportunity to use more environmental friendly and easy-to-handle materials.

Biopolymer binders are attracting increasing attention as alternatives to PVDF due to the large number of functional groups (e.g., hydroxyls and carboxyl), which can lead to good adhesion between active material, conductive additives, and current collector (Versaci et al., 2017; Y.-Y. Zhang et al., 2019). PVDF binds to the electrode components by weak van der Waals forces, which are relatively weak compared to other chemical bonds (Cholewinski et al., 2021). However, polymers such as xanthan gum have plenty of functional groups like hydroxyl groups (-OH) and carboxylic groups (-COOH) that are able to form hydrogen bonds with different components, which are stronger than van der Waals forces (Wang et al., 2022). In addition, the hydrogen bonding is able to "self-heal", hence the ability to accommodate significant volume changes during cycling (Li et al., 2017; S. Li et al., 2021b).

Biopolymers such as guar gum, xanthan gum, and sodium alginate have been used as binders in P2-$Na_{2/3}Ni_{1/3}Mn_{2/3}O_2$ (P2-NNM) (Y.-Y. Zhang et al., 2019), where it was found that electrodes exhibited a better cycling stability and faster rate capability than PVDF. Many biopolymers are water soluble and so are significantly easier to handle than PVDF. There are challenges in applying these to sodium ion batteries. However, as many electrode materials easily take up water due to the larger alkali interlayer spacing (Y. Zhang et al., 2020b; Zhou et al., 2019), it results in the formation of the birnessite-type phase. This phase is detrimental because it can affect morphology where cracks and gliding can be induced in the crystallites, particularly the *00l* plane where the Na layers are located (Zuo et al., 2020). There can also be side reactions between water and electrolyte, as well as blocking diffusion pathways of Na^+ diffusion and leeching of Na from active material to form electrochemically inactive phases (Han et al., 2016; Y. Zhang et al., 2019).

Xanthan gum (XG) is a naturally derived polysaccharide, produced by the bacterium *Xanthomonas campestris*, and is used in food, cosmetic, and pharmaceutical industries (Song et al., 2006). It contains (1,4)-β-D-glucose units with trisaccharide side chains, containing numerous -OH and -COOH groups, and is water soluble. These functional groups act as bonding sites for the active material, carbon, and current collector in electrodes, ensuring good contact and coverage and creating a more comprehensive conduction network (S. Li R.-R. et al., 2021). The structure of XG also provides lone pair of electrons, so it is possible that XG can improve the conduction of electrons in the electrode. Previous work has used XG as a binder to fabricate P2-NNM cells (Y.-Y. Zhang et al., 2019). Initial capacity was measured as 86.7 mAh g^{-1} (between 1.5 and 4.3 V at 1 C), only falling to 75.4 mAh g^{-1} after 300 cycles. When initially showing a similar discharge capacity, cells fabricated using a PVDF binder dropped to 6.8 mAh g^{-1} after 300 cycles, demonstrating the significant advantages afforded by the XG binder. The improvement in cycle stability was attributed to XG facilitating fast Na^+ diffusion and inhibiting manganese dissolution (Y.-Y. Zhang et al., 2019). XG was also used to fabricate $LiFePO_4$ (LFP) cathodes, where this time, the use of XG improved the rate capability: with the XG binder, the discharge capacity was *ca.* 80 mAh g^{-1} *vs. ca.* 50 mAh g^{-1} using PVDF, both at 5 C (He et al., 2017). Similar results were observed with a locust bean gum binder in $LiFePO_4$ and $Li_4Ti_5O_{12}$ (Jakóbczyk et al., 2021). In all of these cases, the biopolymers/polysaccharides reduce both charge transfer resistance and polarization, which is beneficial for cycling at faster rates. Biopolymers, therefore, represent attractive alternatives to the existing organic binders.

Of the Na-ion cathode materials studied to date, one of the most promising is P2-$Na_{2/3}Ni_{2/3}Mn_{2/3}O_2$ (P2-NNM). NNM can also form the P3-type structure, although this can be difficult to access *via* traditional synthetic methods (Lee et al., 2017; Wang et al., 2013; Wen et al., 2015; L. Zhang et al., 2020b). Both P2- and P3-NNM structures, shown in Supplementary Figure S1 using Delmas notation (Delmas et al., 1980), show negligible structural change on storage under ambient conditions or after immersion in water (Y. Zhang et al., 2020b; Y.-Y. Zhang et al., 2019; Zhou et al., 2019), making them good candidates for use with the water-based binders. As P3-NNM can be synthesized at lower temperatures, it is a potentially more sustainable alternative to P2-NNM (Lee et al., 2017; L. Zhang et al., 2020b; Zilinskaite et al., 2018), with equivalent or a slightly better specific capacity (Wen et al., 2015; L. Zhang et al., 2020b; Zheng et al., 2018).

In this study, we investigated the stability of P3-NNM under ambient conditions and understood the practical requirements for controlling/removing hydrated phases, as a precursor to use with the water-soluble binders. We then compared the cycling stability and rate capability of P3-NNM electrodes prepared using XG and PVDF. It was found that the choice of the binder had a negligible impact on the measured capacity or cycling stability, indicating that water exposure during electrode preparation with XG does not negatively impact electrochemical performance.

Methods

Materials and synthesis

P3-NNM was synthesized by dextran biotemplating, as reported previously (Zilinskaite et al., 2018). The reagents were obtained from Sigma-Aldrich (UK) with 98+% purity and used without further treatment. P3-NNM was synthesized by first mixing stoichiometric amounts of sodium acetate, nickel acetate tetrahydrate, and manganese acetate tetrahydrate, dissolved in distilled water. Dextran (M_r = 70,000) was then added to the solution, which was mixed until dextran had dissolved and then dried at 80°C in air atmosphere. The resulting amorphous metal ion-organic composite was calcined in a muffle furnace at a heating rate of 10°C/min to 650°C, held for 2 h in an air atmosphere.

Characterization

X-ray diffraction (XRD) used a PANalytical Aeris powder diffractometer with Ni-filtered Cu Kα radiation (λ = 1.5406 Å). Phase analysis used the International Centre for Diffraction Data PDF-4+ database, 2020 edition, and SIeve + software. The samples for scanning electron microscopy (SEM) were prepared by using affixing powder on a carbon tape and sputter-coated with a thin layer of gold. SEM was also conducted on prepared electrodes, which were also affixed onto the tape with no sputtering of gold. The samples were investigated using a Philips Inspect F50 SEM. Pawley refinement was conducted on HighScore software (PANalytical) to calculate the lattice parameters. The data were calibrated for peak position errors using the NIST 640e silicon standard reference material.

Electrochemistry

Electrodes were prepared by mixing 80 wt% active material, 10 wt% binder, and 10 wt% carbon (Timical Super C65, MTI). For the PVDF binder, sufficient volume of 1-methyl-2-pyrrolidone (anhydrous 99.5%, Sigma-Aldrich) was added and mixed thoroughly using a Thinky ARE-250 Mixer until the PVDF was fully dissolved. For xanthan gum, the powders were instead mixed by pestle and mortar with distilled water. The resulting slurries were then cast onto carbon-coated aluminum foil using a micrometer adjustable doctor blade. The coated foils were dried under vacuum at 80°C, before calendaring using a rolling mill (MTI, MSK-HRP-MR100DC).

Stainless steel coin cells (2032) were assembled in a dry Ar-filled glovebox (MBraun). The cells were constructed using the following layering sequence: a stainless steel spacer was placed first, then a freshly punched sodium disc rolled from sodium ingot (99.8%, Alfa Aesar), then a glass fiber separator (GF/F Whatman) soaked in electrolyte solution (1.0 mol L^{-1} $NaPF_6$ in EC: DEC (1:1 v/v %), Fluorochem), and then the working electrode of interest, before being crimped closed.

Galvanostatic tests used a Maccor Series 4000 Battery Cycler in a 25°C climate-controlled chamber. The cells were first left under open circuit conditions to rest for 4 h before cycling at various voltage ranges (between 1.5 and 4.5 V) and rates (between 0.1 and 2 C) *vs.* Na/Na^+. Cyclic voltammetry (CV) was conducted using a Maccor Series 4300 Battery Cycler at a scan rate of 0.1 mV s^{-1} over two potential ranges, from 2.0 to 4.5 V and 1.5 to 4.1 V. All references to potential and voltage are relative to the Na/Na^+ reference.

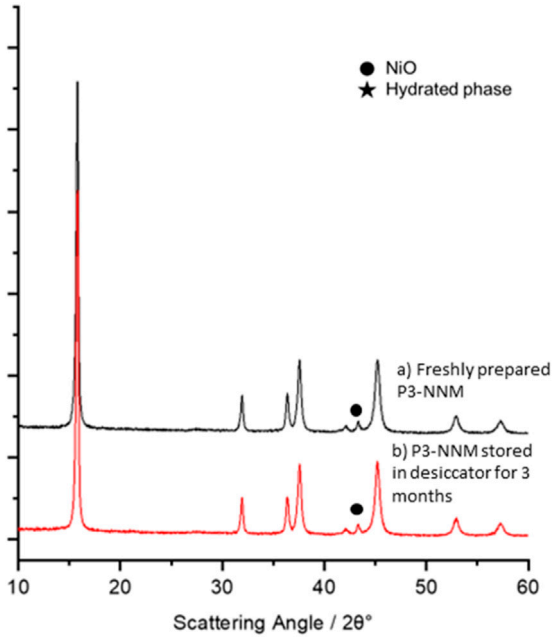

FIGURE 1
XRD data for P3-NNM **(A)** freshly prepared (black) and **(B)** after storage in a desiccator for 3 months (red). Secondary phases are indicated using a filled circle (NiO) or star (hydrated phase) symbol.

Results and discussion

Before preparing electrodes, the stability of the as-prepared P3-NNM powder in ambient and near ambient conditions was tested. Comparison of X-ray diffraction data for the freshly prepared (Figure 1A) and stored (3-months in a desiccator, Figure 1B) specimens show no obvious structural changes nor the development of additional Bragg reflections, indicating that there was no detectable formation of hydrated phases following long-term storage of specimens under relatively dry conditions. In each instance, the observed Bragg reflections were indexed to

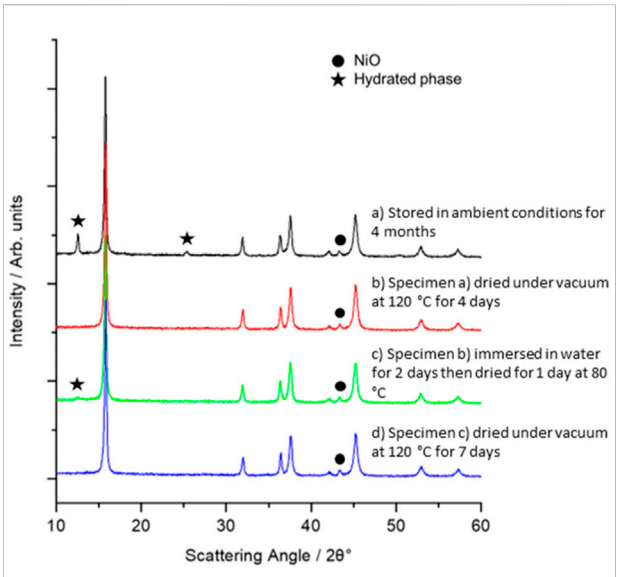

FIGURE 2
XRD data for P3-NNM after **(A)** storage in a cupboard for 4 months (black), **(B)** dried in a vacuum oven for 4 days at 120°C (red), **(C)** immersed in water for 2 days and dried for 1 day at 80°C (green), and **(D)** then finally dried in a vacuum oven for 7 days at 120°C (blue). Additional Bragg reflections from secondary phases are indicated using a filled circle (NiO) or star (hydrated phase) symbol.

P3-NNM (PDF card 04-016-7123) with a small quantity of NiO, Figure 1, typical in synthetic studies of materials with this or similar compositions (Lee et al., 2017; Wang et al., 2016; J. Zhang et al., 2019). Longer-term ambient storage, outside a desiccator where humidity is greater was also investigated. Figure 2A shows the XRD pattern of P3-NNM stored in ambient conditions for 4 months, and additional Bragg reflections of low intensity are observed here, indexed to the formation of a hydrated phase (Zuo et al., 2020). This is indicative of water molecules inserting into the structure, increasing the *c*-axis layer spacing forming a birnessite-type phase (Zuo et al., 2020), similar to the previous work (Lu and Dahn, 2001; Y. Zhang et al., 2020b). The ratio of the hydrated phase to the main phase in our work, however, is lower than that reported previously, indicating that P3-NNM may have a better ambient stability than other reported compositions, (e.g., $Na_{2/3}Fe_{1/9}Ni_{1/6}Mn_{2/3}O_2$, $Na_{2/3}Co_{1/9}Ni_{1/6}Mn_{2/3}O_2$, and $Na_{2/3}MnO_2$) (Y. Zhang et al., 2020b, 2019; Zuo et al., 2020).

For use with an XG binder, the electrode powders need to be stable on immersion in water (*vs.* long term storage). Figure 2B shows the XRD pattern of pristine, dry P3-NNM powder (stored under vacuum at 120°C), followed by immersion in water and subsequent drying at 80°C in air, as shown in Figure 2C. Here, we observe that small hydration peaks do emerge, in contrast to previous work which showed P3-NNM to be stable when immersed in water (Zhou et al., 2019). Hence, it is important to dry the material at higher temperatures and under vacuum to ensure that it is fully dehydrated. Pawley refinement was conducted on a specimen that was immersed in water and then dried at 80°C, as shown in Supplementary Figure S2. Lattice parameters were obtained for P3-NNM and its hydrated analogs, as shown in Supplementary Table S1. There was minimal difference in the *a*-axis, with values of 2.88 and 2.89 Å, respectively. The hydrated P3-NNM has a *c*-axis of 20.93 Å, which is significantly larger than the pristine layered oxide, (16.85 Å, Supplementary Table S1). The significant shift of the 00*l* plane to lower angles is due to the insertion of water molecules in the Na layer, as found in many other similar materials (Lu and Dahn, 2001; Y. Zhang et al., 2020b; Zuo et al., 2020).

There are various factors that can affect the stability of these layered structures in ambient conditions. In P2-NNM, it has been shown that superlattice ordering prevents water intercalation due to strong coupling between adjacent TmO_2 layers and surface adsorption energy of water that is dependent on Tm (Lu and Dahn, 2001; Y. Zhang et al., 2020b). The superlattice structure occurs when there is ordering of Ni and Mn in the Tm layers. Such ordering is possible in the P3 polymorph due to the 1/3:2/3 Ni to Mn ratio (Lu et al., 2000), hence giving a possible reason for the stability of P3-NNM in aqueous conditions (Zhou et al., 2019). Superlattice ordering can sometimes be resolved using X-rays. P2-type materials such as P2-$Na_{2/3}Ni_{1/3-x}Cu_xMn_{2/3}O_2$ and P2-$Na_{2/3}Ni_{1/3}Mn_{2/3}O_2$ have exhibited peaks *ca.* 27.2° and 28.3° 2θ (Cu Kα radiation), which were attributed to in-plane sodium/vacancy ordering (Zheng et al., 2017; Dang et al., 2019), which is affected by ordering of transition metals in the TM layers, as Na prefers to occupy sites around Ni (L. Zhang et al., 2020a). There are no obvious signs of small peaks in this region or other additional peaks in Figures 1, 2. However, since Ni and Mn can be difficult to differentiate using X-rays, superlattice ordering may require neutron diffraction to be fully resolved (Lu et al., 2000).

Superlattice ordering can be destroyed by substituting other elements such as Co and Fe, causing the material to be less stable in air and/or water (Lu and Dahn, 2001). Some materials that demonstrate water stability in ambient conditions do not necessarily have superlattice ordering. Alternatively, materials that have shown water stability have Mn valency close to +4 or those with relatively higher redox potentials or high degree of crystallinity (Zuo et al., 2020). There has been a study on reducing superlattice ordering of P3-NNM, which was achieved by the synthesis method used; however, water stability was not investigated (L. Zhang et al., 2020b). In this case, we postulate that biotemplated P3-NNM may have a disordered TM arrangement, or is less crystalline due to the short calcination time. Hence, small amounts of the hydrated phase forms after a while in ambient conditions. With longer calcination time, crystallinity and TM ordering may increase, which may lead to better stability in ambient and water conditions.

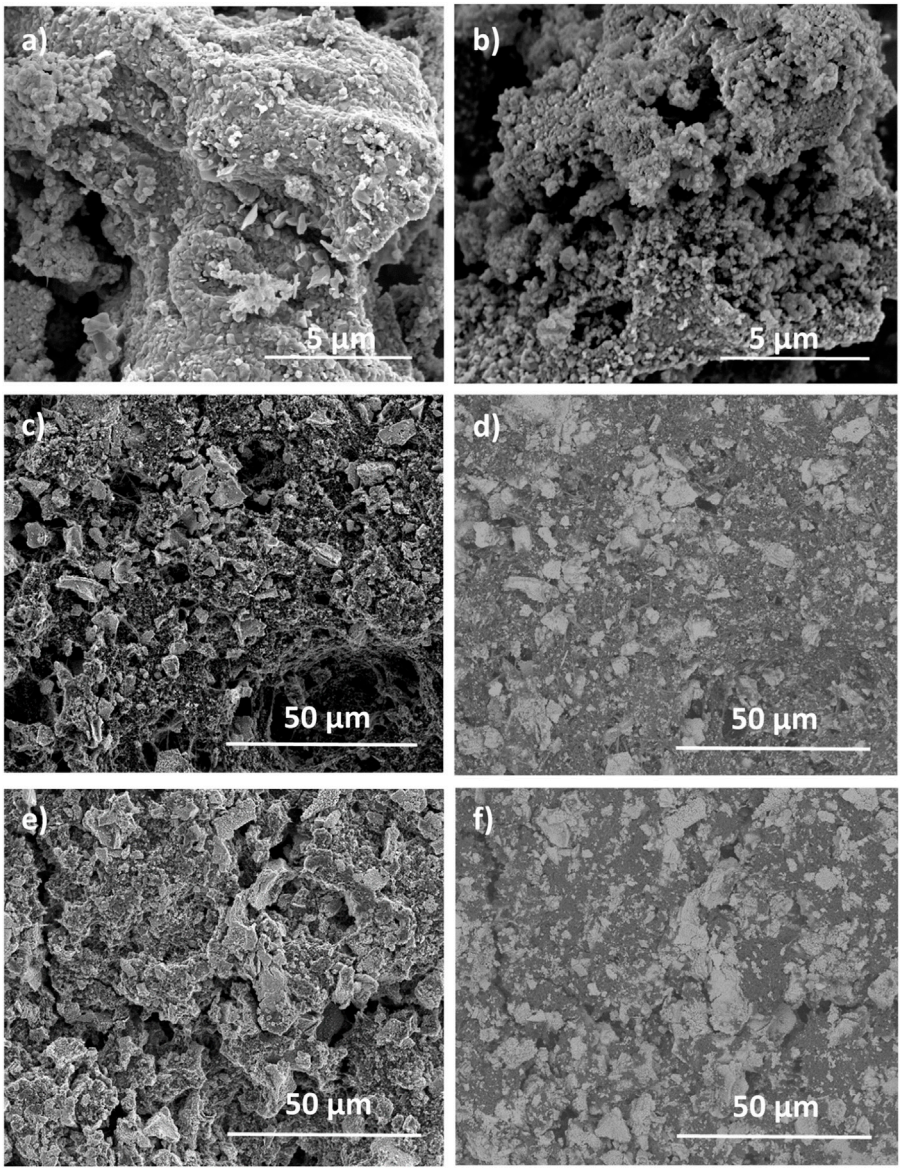

FIGURE 3
SEM images of P3-NMM **(A)** freshly prepared **(B)** powder immersed in water and then dried at 80°C to remove excess water before drying at 120°C under vacuum; **(C)** secondary electron image of a P3-NNM cathode prepared using PVDF and **(D)** corresponding BSE image; **(E)** secondary electron image of a P3-NNM cathode prepared using XG and **(F)** corresponding BSE image.

It is possible to convert the hydrated phase back into the original P3-NNM phase, as demonstrated in similar materials (Lu and Dahn, 2001). After drying in a vacuum oven at 120°C, Figure 2D shows that the reflection(s) indexed to the hydrated phase have been completely removed, and it appears that the pristine cathode material is recovered. First, this indicates that the hydration of P3-NNM appears to be fully reversible and second gives insight into the conditions required to use water-based binders with P3-NNM, that is, once the binder is incorporated, the electrode tapes must be dried under vacuum at ≥ 120°C to fully dehydrate.

SEM was conducted to examine the impact of water on crystallite morphology. Figures 3A,B show the SEM images of P3-NNM powder specimens as prepared (3a) and following immersion in water and subsequent drying at 80°C until excess water has evaporated before vacuum drying at 120°C (b). There is no obvious sign of intragrain cracks or layer glide, which has been found in other materials after exposure to water (Zuo et al., 2020). The higher magnification images in

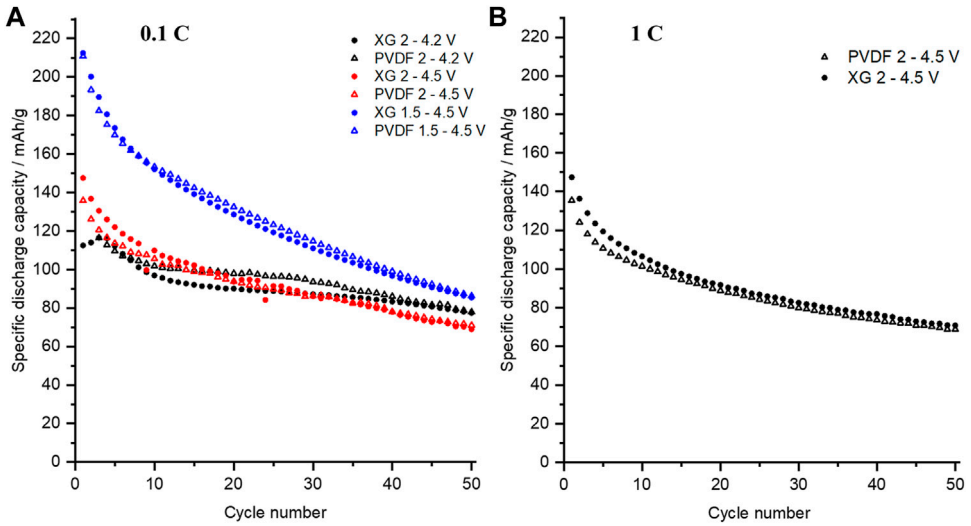

FIGURE 4
Cycling performance on P3-NNM with either the XG or PVDF binder **(A)** cycled at different voltages at 0.1 C and **(B)** at 1 C.

Supplementary Figure S3 also show no observable difference pre- and post-water immersion. If water intercalation did any lasting damage, to the extent that electrochemical performance would be affected, it would likely be evident even after drying under vacuum at 120°C. As shown in our previous study, the biotemplating synthetic process produces agglomerated particles of P3-NNM with individual average particle sizes in the range of 100–200 nm (Zilinskaite et al., 2018), which can be observed in Figures 3A,B. Such morphologies have been found in other dextran-templated materials (Walsh et al., 2003). Particle agglomeration has been shown to increased charge transfer resistances due to the abundance of particle–particle interface (Hu et al., 2004; Y. Liu et al., 2020b; Stein et al., 2016), and so this may have a deleterious impact on electrochemical performance. Figures 3C,D show secondary and backscattered electron (BSE) images of the cathode prepared using the PVDF binder. Figure 3C clearly shows evidence of particle agglomeration, and regions of lighter contrast in the BSE image shown in Figure 3D can be attributed to the P3-NNM phase with darker regions to the carbon and binder. The same agglomeration is seen when the sample is prepared using XG in Figures 3E,F, indicating that the two binders are forming electrodes with similar architecture. This shows that agglomeration is due to the synthesis method rather than electrode fabrication. There are cracks in both the cathodes on the macroscale and are likely due to over calendaring and/or during sample preparation for SEM. Since there are fairly large agglomerates, when the electrodes are being calendared, crack propagation is likely to occur and there is nothing to keep the particles together. This is something that needs optimizing in terms of calendaring and potentially weight fraction of binder, as XG is more viscous than PVDF (He et al., 2017).

Cells containing working electrodes fabricated using either PVDF or xanthan gum as the binder were cycled galvanostatically over 50 charge–discharge cycles at rates of 0.1 C over the potential range 2–4.2 V (as per common testing regimes reported in the literature for P3-NNM) or over extended ranges to lower (1.5 V) and/or higher (4.5 V) potential limits at 0.1 and/or 1 C charge rates in order to accentuate the effects from any degradation mechanisms, with the resulting discharge capacities plotted in Figures 4A,B. Irrespective of voltage range, there is no significant difference in the cycling stability between cells that use XG or the PVDF binder. At 2.0–4.2 V, initial discharge capacities of *ca.* 115 mAh g^{-1} were observed. In both cases when cycled between 1.5 and 4.5 V, P3-NNM exhibited initial discharge capacities in excess of 200 mAh g^{-1}, higher than the theoretical capacity for P3-NNM of 173 mAh g^{-1}, irrespective of the binder. This higher measured capacity could be due to a variety of additional contributions such as oxygen redox which is normally seen above 4 V (Kim et al., 2020; Wang et al., 2019; Y. Zhang et al., 2020a) and Mn redox below 2 V (Hong et al., 2019; Liu et al., 2019), both of which have been seen in similar materials but not thoroughly studied in P3-NNM. This high initial capacity is also observed for cells cycled between 2.0 and 4.5 V at a faster rate of 1 C, as shown in Figure 4B. The higher capacity could also be due to electrolyte degradation, where oxidation of $NaPF_6$ in EC: DEC (1:1 v/v) is seen to start at 3.7 V for the first few cycles (Ould et al., 2021).

Figure 5A shows the voltage profiles of P3-NNM with XG and Figure 5B with PVDF. Both profiles show the same plateaus

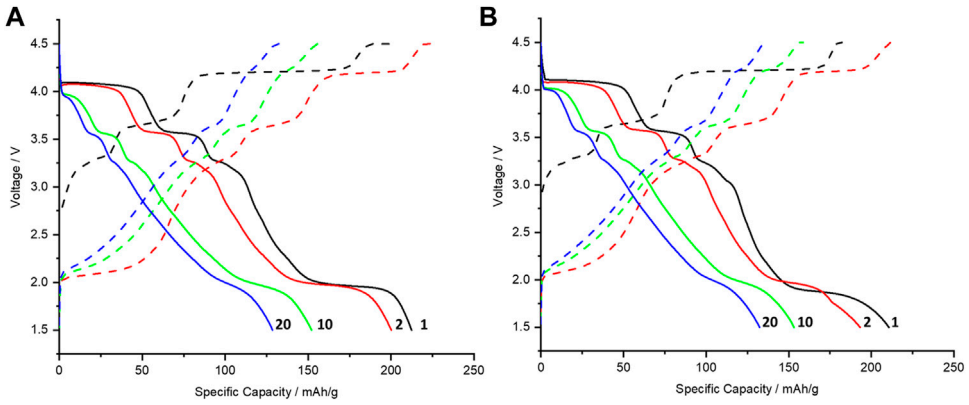

FIGURE 5
Voltage profiles of the first, second, tenth, and twentieth galvanostatic charges (dashed lines) and discharges (solid lines) for biotemplated P3-NNM cycled at 0.1 C between 1.5 and 4.5 V, where the working electrode was made using **(A)** XG and **(B)** PVDF binders.

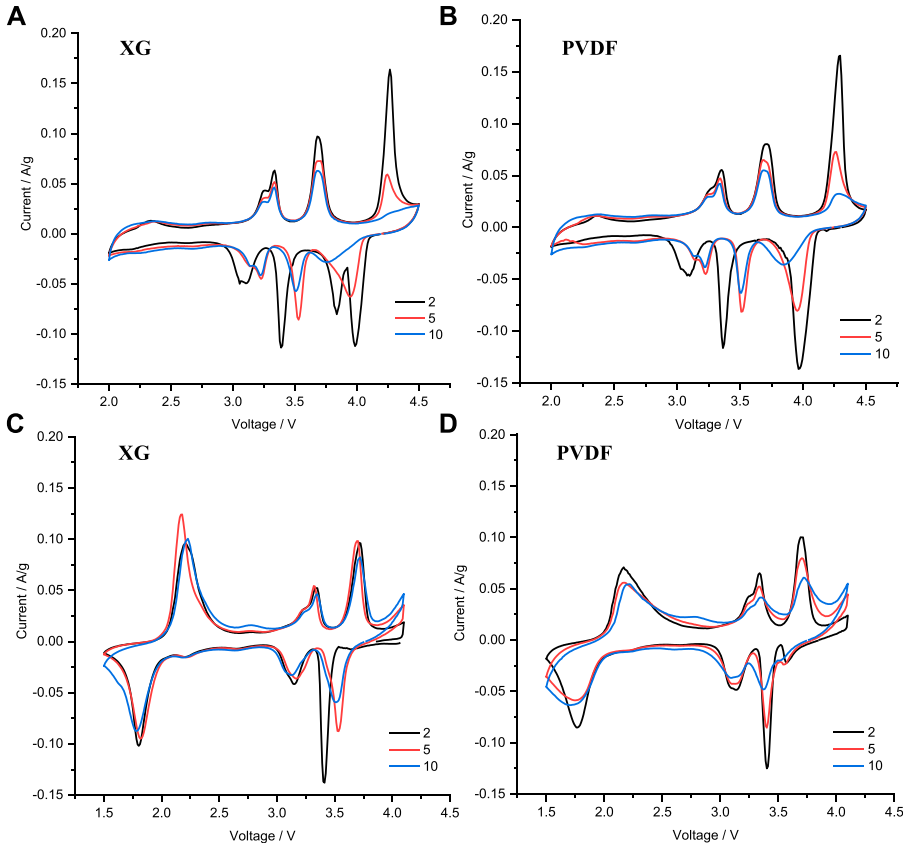

FIGURE 6
Cyclic voltammograms recorded at 0.1 mV s^{-1} for cells containing P3-NNM with **(A,C)** XG and **(B,D)** PVDF. Cells were cycled between **(A,B)** 2.0 and 4.5 V or between **(C,D)** 1.5 and 4.1 V.

on discharge at *ca.* 1.9, 3.3, 3.6, and 4.1 V. The most prominent plateaus are around 1.9 and 4.1 V; however, they quickly fade upon subsequent cycles. A plateau at 4.1 V upon charge can be attributed to the P3-O3 phase transition (J. Liu et al., 2020a; Shi et al., 2021), associated with the shrinkage of the *a-b* plane of TmO_2 layers and at 1.9 V upon discharge is due to a P3-P3' transition, with an increase in number of Na atoms (Zhang, 2019). The P3-O3 phase transition is associated with a large change in the unit cell volume; however, effects of this phase transition are not as well-understood as the P2-O2 transition in P2-NNM (Guo et al., 2016). In P2-NNM, the phase transition at high voltages has been associated with intergranular cracking (K. Wang et al., 2018), as well as sluggish Na^+-ion migration kinetics as the diffusion coefficient decreases in the O2-type phase (Liu et al., 2019). It may be because similar phenomena occur during the P3-O3 phase transition as well (Zhang, 2019). The other plateaus at 3.3 and 3.6 V can be attributed to different Na^+/vacancy ordering, as noted for the P2-NNM polymorph in the literature (Lee et al., 2013; P. F. Wang et al., 2018). Both the cathodes prepared with XG and PVDF show a similar rate of plateau degradation.

Cyclic voltammograms were collected for cells using electrodes made with XG (Figures 6A,C) and PVDF (Figures 6B,D) binders. The findings are broadly similar, regardless of binder choice, with five main redox pairs at the anodic/cathodic voltages of around 4.3/4.0, 3.7/3.4, 3.3/3.1, 3.2/3.0, and 2.2/1.8 V. The samples prepared with XG have an additional cathodic peak at 3.8 V when cycled between 2.0 and 4.5 V, as shown in Figure 6A, which is not observed in the samples containing PVDF, as shown in Figure 6C. This could be due to water, causing side reactions with the electrolyte which needs to be confirmed. In Figure 6D, NNM-PVDF shows an additional small cathodic peak at 3.6 V when cycled between 1.5 and 4.1 V, which decreases in intensity upon subsequent cycles, although the cause of this peak is also unknown. It is apparent here that the CV peaks at 4.3/4.0 V diminish with repeated cycling to 4.5 V, and so these factors could be contributing to fast capacity fade, as shown in Figure 4A (blue data points). Further investigation is needed to determine the degradation mechanism at higher voltages for P3-NNM, to deconvolute potential oxygen redox and the P3-O3 phase transition. This is because oxygen redox and such phase transitions occur at similar potentials, in least for the P2 form of this composition and for other P3 structures with similar stoichiometries (Kim et al., 2020; J. Liu et al., 2020; Zhang, 2019; Y. Zhang et al., 2020a).

The three pairs of peaks at intermediate potentials all show similar behavior irrespective of the binder and have all been associated in reported studies with the $Ni^{2+}/Ni^{3+}/Ni^{4+}$ redox activity for P2-NNM (Lee et al., 2017; Wang et al., 2019), and when this is less well-studied for the P3 polymorph, it is reasonable that similar behavior is followed. The redox activity occurring at lower potentials, *ca.* 2 V, can be attributed to the $Mn^{3+/4+}$ redox couple, similar to reports on

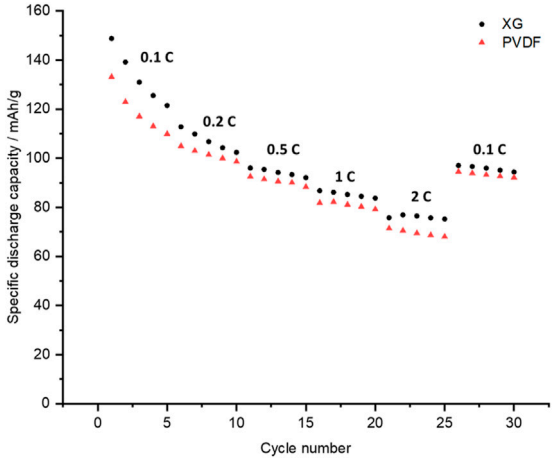

FIGURE 7
Rate capability of P3-NNM when using xanthum gum (black circles) or PVDF (red triangles) as the binder. Cells are cycled galvanostatically between 2.0 and 4.5 V.

P2-NNM (Gutierrez et al., 2018; Wen et al., 2015; Y.-Y. Zhang et al., 2019). In our experiments, with an extended lower voltage cutoff (1.5 V), greater initial discharge capacities were observed, along with faster capacity fading, as shown in Figure 4A. This could be due to the formation of Jahn–Teller active Mn^{3+}, which may lead to local structural distortions and also is prone to disproportion to form Mn^{2+} and Mn^{4+}, where the former is liable to dissolution into the electrolyte (Wen et al., 2015; Hong et al., 2019). With significant volume change, fresh surface can be exposed, where further dissolution of Mn can occur, leading to poor cycle stability (Hong et al., 2019; K. Wang et al., 2018). This is an ongoing discussion, however, with some contradictory results in previously published studies. For example, some studies on P3-NNM have shown no Mn redox activity at low potentials, while the $Mn^{3+/4+}$ redox activity has been reported in work on other very similar compositions, such as P3-$Na_{0.67}Ni_{0.2}Mn_{0.8}O_2$.(Zhang, 2019) (Kim et al., 2020). Further investigation is merited in this area.

Figure 7 compares the rate capability of cathodes with different binders cycled between 2.0 and 4.5 V. Cells using each type of binder showed comparable performance at different C-rates, although discharge capacities are slightly higher for the XG-bound electrodes at all charge rates, especially at 2 C. This could be due to XG potentially aiding conduction of electrons, thus reducing charge transfer resistance (Y.-Y. Zhang et al., 2019). The full potential of XG may not be realized here as the SEM images show fairly large agglomerates. This leads to increased charge transfer resistance where there are particles that are not in contact with the conductive material and the binder. This can affect the kinetics in battery materials as there can be poor conductivity and transport on the alkali ions

(X. Zhang et al., 2019). Because of this, aggregation has been shown to negatively impact rate capability (Stein et al., 2016; X. Zhang et al., 2019).

From the data presented, it is clear that exposure to water does not have negative impact on key metrics of electrochemical performance for the P3-NNM powder. The use of either PVDF or XG as binders leads to comparable cycling performance and stability and similar rate capability, regardless of the voltage range of cycling. P3-NNM is, therefore, a good candidate for water-based binders, such as xanthan gum, which offers significant possible benefits in handling and safety through the elimination of toxic solvents such as NMP, without compromising electrochemical performance.

Conclusion

We have demonstrated that P3-$Na_{2/3}Ni_{1/3}Mn_{2/3}O_2$ (P3-NNM) is relatively stable under standard ambient conditions and on immersion on water and that while the limited formation of hydrated phases may occur, these are easily reversible on mild heating under vacuum, with no impact on electrochemical performance. This suggests that P3-NNM is a suitable candidate material for the development of water-based binders. Electrodes using the xanthan gum binder P3-NNM show similar microstructures and comparable performance to those fabricated using PVDF, which requires dissolution in 1-methyl-2-pyrrolidone, generally considered to be toxic and difficult to handle. On cycling at 0.1 C between 2.0 and 4.2 V, both the electrodes prepared with XG and PVDF exhibited initial discharge capacities of *ca.* 115 mAh g^{-1} and after 50 cycles exhibited a capacity of 77 mAh g^{-1}. When the voltage range was extended to 1.5–4.5 V, both exhibited initial discharge capacities of *ca.* 210 mAh g^{-1}, although the theoretical capacity is 173 mAh g^{-1}, with poor capacity retention (41%) after 50 cycles, likely attributable to oxygen and Mn redox and electrolyte oxidation. Xanthan gum represents a realistic and easily implementable water-based binder for P3-NNM, offering a timely pathway toward improved sustainability of battery fabrication without the loss of performance.

Data availability statement

The raw data supporting the conclusion of this article will be made available by the authors, without undue reservation.

Author contributions

SZ designed and synthesized samples, performed experiments, and conducted data analysis. All authors wrote the manuscript and contributed to general discussion and manuscript revision.

Funding

This work has been funded by EPSRC *via* grant EP/L016818/1 which funds the Centre for Doctoral Training in Energy Storage and its Applications, International Consortium of Nanomaterials, Lloyds Register Foundation, and the Royal Academy of Engineering.

Acknowledgments

The authors wish to acknowledge the Henry Royce Institute for Advanced Materials, funded through EPSRC grants EP/R00661X/1, EP/S019367/1, EP/P02470X/1 and EP/P025285/1, and EP/V034804/1, for access to the X-ray diffraction facility, PANalytical Aeris, and Maccor Series 4300 Battery Tester at Royce at the University of Sheffield. They also thank the Sorby Centre for Electron Microscopy for the access to the Philips Inspect F50 for SEM imaging. RB acknowledges that the project was supported by the Lloyd's Register Foundation and Royal Academy of Engineering under the Research Fellowships scheme.

Conflict of interest

The authors declare that the research was conducted in the absence of any commercial or financial relationships that could be construed as a potential conflict of interest.

Publisher's note

Supplementary material

The Supplementary Material for this article can be found online at: https://www.frontiersin.org/articles/10.3389/fenrg.2022.909486/full#supplementary-material

References

Chen, Z., Christensen, L., and Dahn, J. R. (2003). Comparison of PVDF and PVDF-TFE-P as binders for electrode materials showing large volume changes in lithium-ion batteries. *J. Electrochem. Soc.* 150, A1073. doi:10.1149/1.1586922

Cholewinski, A., Si, P., Uceda, M., Pope, M., and Zhao, B. (2021). Polymer binders: Characterization and development toward aqueous electrode fabrication for sustainability. *Polym. (Basel)* 13, 631. doi:10.3390/polym13040631

Dang, R., Chen, M., Li, Q., Wu, K., Lee, Y. L., Hu, Z., et al. (2019). Na+-Conductive $Na_2Ti_3O_7$-modified P2-type Na2/3Ni1/3Mn2/3O2 *via* a smart *in situ* coating approach: Suppressing Na+/Vacancy ordering and P2-O2 phase transition. *ACS Appl. Mat. Interfaces* 11, 856–864. doi:10.1021/acsami.8b17976

Delmas, C., Fouassier, C., and Hagenmuller, P. (1980). Structural classification and properties of the layered oxides. *Phys. B+C* 99B, 81–85. doi:10.1016/0378-4363(80)90214-4

Guerfi, A., Kaneko, M., Petitclerc, M., Mori, M., and Zaghib, K. (2007). $LiFePO_4$ water-soluble binder electrode for Li-ion batteries. *J. Power Sources* 163, 1047–1052. doi:10.1016/J.JPOWSOUR.2006.09.067

Guo, S., Sun, Y., Yi, J., Zhu, K., Liu, P., Zhu, Y., et al. (2016). Understanding sodium-ion diffusion in layered P2 and P3 oxides *via* experiments and first-principles calculations: A bridge between crystal structure and electrochemical performance. *NPG Asia Mat.* 8, 266–274. doi:10.1038/am.2016.53

Gutierrez, A., Dose, W. M., Borkiewicz, O., Guo, F., Avdeev, M., Kim, S., et al. (2018). On disrupting the Na^+-Ion/Vacancy ordering in P2-type Sodium–Manganese–Nickel oxide cathodes for Na^+-Ion batteries. *J. Phys. Chem. C* 122, 23251–23260. doi:10.1021/acs.jpcc.8b05537

Han, M. H., Sharma, N., Gonzalo, E., Pramudita, J. C., Brand, H. E. A., López Del Amo, J. M., et al. (2016). Moisture exposed layered oxide electrodes as Na-ion battery cathodes. *J. Mat. Chem. A* 4, 18963–18975. doi:10.1039/C6TA07950D

He, J., Zhong, H., Wang, J., and Zhang, L. (2017). Investigation on xanthan gum as novel water soluble binder for $LiFePO_4$ cathode in lithium-ion batteries. *J. Alloys Compd.* 714, 409–418. doi:10.1016/J.JALLCOM.2017.04.238

Hong, J. H., Wang, M. Y., Du, Y. Y., Deng, L., and He, G. (2019). The role of Zn substitution in P2-type $Na_{0.67}Ni_{0.23}Zn_{0.1}Mn_{0.67}O_2$ cathode for inhibiting the phase transition at high potential and dissolution of manganese at low potential. *J. Mat. Sci. Mat. Electron.* 30, 4006–4013. doi:10.1007/s10854-019-00687-5

Hu, Y., Doeff, M. M., Kostecki, R., and Fiñones, R. (2004). Electrochemical performance of sol-gel synthesized $LiFePO_4$ in lithium batteries. *J. Electrochem. Soc.* 151, A1279–A1285. doi:10.1149/1.1768546

Jakóbczyk, P., Bartmański, M., and Rudnicka, E. (2021). Locust bean gum as green and water-soluble binder for $LiFePO_4$ and $Li_4Ti_5O_{12}$ electrodes. *J. Appl. Electrochem.* 51, 359–371. doi:10.1007/s10800-020-01496-z

Kim, E. J., Ma, L. A., Duda, L. C., Pickup, D. M., Chadwick, A. v., Younesi, R., et al. (2020). Oxygen redox activity through a reductive coupling mechanism in the P3-type nickel-doped sodium manganese oxide. *ACS Appl. Energy Mat.* 3, 184–191. doi:10.1021/acsaem.9b02171

Lee, D. H., Xu, J., and Meng, Y. S. (2013). An advanced cathode for Na-ion batteries with high rate and excellent structural stability. *Phys. Chem. Chem. Phys.* 15, 3304–3312. doi:10.1039/c2cp44467d

Lee, S. Y., Kim, J. H., and Kang, Y. C. (2017). Electrochemical properties of P2-type $Na_{2/3}Ni_{1/3}Mn_{2/3}O_2$ plates synthesized by spray pyrolysis process for sodium-ion batteries. *Electrochim. Acta* 225, 86–92. doi:10.1016/j.electacta.2016.11.141

Li, J. T., Wu, Z. Y., Lu, Y. Q., Zhou, Y., Huang, Q. S., Huang, L., et al. (2017). Water soluble binder, an electrochemical performance booster for electrode materials with high energy density. *Adv. Energy Mat.* 7, 1701185. doi:10.1002/AENM.201701185

Li, R.-R., Yang, Z., He, X.-X., Liu, X.-H., Zhang, H., Gao, Y., et al. (2021a). Binders for sodium-ion batteries: Progress, challenges and strategies. *Chem. Commun.* 57, 12406–12416. doi:10.1039/d1cc04563f

Li, S., Wu, Z.-G., Liu, Y.-M., Yang, Z.-W., Wang, K., Liu, Y.-X., et al. (2021b). A compared investigation of different biogum polymer binders for silicon anode of lithium-ion batteries. *Ionics (Kiel)* 27, 1829–1836. doi:10.1007/s11581-021-03944-y/Published

Lingappan, N., Kong, L., and Pecht, M. (2021). The significance of aqueous binders in lithium-ion batteries. *Renew. Sustain. Energy Rev.* 147, 111227. doi:10.1016/J.RSER.2021.111227

Liu, J., Didier, C., Sale, M., Sharma, N., Guo, Z., Peterson, V. K., et al. (2020a). Elucidation of the high-voltage phase in the layered sodium ion battery cathode material P_3–Na 0.5 Ni 0.25 Mn 0.75 O 2. *J. Mat. Chem. A Mat.* 8, 21151–21162. doi:10.1039/D0TA06600A

Liu, Q., Hu, Z., Chen, M., Zou, C., Jin, H., Wang, S., et al. (2019). P2-type $Na_{2/3}Ni_{1/3}Mn_{2/3}O_2$ as a cathode material with high-rate and long-life for sodium ion storage. *J. Mat. Chem. A* 7, 9215–9221. doi:10.1039/c8ta11927a

Liu, Y., Shen, Q., Zhao, X., Zhang, J., Liu, X., Wang, T., et al. (2020b). Hierarchical engineering of porous P2-$Na_{2/3}Ni_{1/3}Mn_{2/3}O_2$ nanofibers assembled by nanoparticles enables superior sodium-ion storage cathodes. *Adv. Funct. Mat.* 30, 1907837. doi:10.1002/adfm.201907837

Liu, Z., Shen, J., Feng, S., Huang, Y., Wu, D., Li, F., et al. (2021). Ultralow volume change of P2-type layered oxide cathode for Na-ion batteries with controlled phase transition by regulating distribution of Na^+. *Angew. Chem. Int. Ed.* 60, 20960–20969. doi:10.1002/ANIE.202108109

Lu, Z., and Dahn, J. R. (2001). Intercalation of water in P2, T2 and O2 structure az $[Co_xNi_{1/3-x}Mn_{2/3}]O_2$. *Chem. Mat.* 13, 1252–1257. doi:10.1021/cm000721x

Lu, Z., Donaberger, R. A., and Dahn, J. R. (2000). Superlattice ordering of Mn, Ni and Co in layered alkali transition metal oxides with P2, P3 and O3 structures. *Chem. Mat.* 12, 3583–3590. doi:10.1021/cm000359m

Ould, D. M. C., Menkin, S., O'Keefe, C. A., Coowar, F., Barker, J., Grey, C. P., et al. (2021). New route to battery grade $NaPF_6$ for Na-ion batteries: Expanding the accessible concentration. *Angew. Chem. Int. Ed.* 60, 24882–24887. doi:10.1002/ANIE.202111215

Patra, J., Rath, P. C., Li, C., Kao, H. M., Wang, F. M., Li, J., et al. (2018). A water-soluble NaCMC/NaPAA binder for exceptional improvement of sodium-ion batteries with an SnO_2-ordered mesoporous carbon anode. *ChemSusChem* 11, 3923–3931. doi:10.1002/CSSC.201801962

Shi, Y., Zhang, Z., Jiang, P., Gao, A., Li, K., Zhang, Q., et al. (2021). Unlocking the potential of P3 structure for practical Sodium-ion batteries by fabricating zero strain framework for Na+ intercalation. *Energy Storage Mater.* 37, 354–362. doi:10.1016/j.ensm.2021.02.020

Song, B., Hu, E., Liu, J., Zhang, Y., Yang, X. Q., Nanda, J., et al. (2019). A novel P3-type $Na_{2/3}Mg_{1/3}Mn_{2/3}O_2$ as high capacity sodium-ion cathode using reversible oxygen redox. *J. Mat. Chem. A* 7, 1491–1498. doi:10.1039/c8ta09422e

Song, K. W., Kim, Y. S., and Chang, G. S. (2006). Rheology of concentrated xanthan gum solutions: Steady shear flow behavior. *Fibers Polym.* 7, 129–138. doi:10.1007/BF02908257

Stein, M., Chen, C. F., Mullings, M., Jaime, D., Zaleski, A., Mukherjee, P. P., et al. (2016). Probing the effect of high energy ball milling on the structure and properties of $LiNi_{1/3}Mn_{1/3}Co_{1/3}O_2$ cathodes for Li-ion batteries. *J. Electrochem. Energy Convers. Storage* 13, 031001. doi:10.1115/1.4034755

Versaci, D., Nasi, R., Zubair, U., Amici, J., Sgroi, M., Dumitrescu, M. A., et al. (2017). New eco-friendly low-cost binders for Li-ion anodes. *J. Solid State Electrochem.* 21, 3429–3435. doi:10.1007/s10008-017-3665-5

Walsh, D., Arcelli, L., Ikoma, T., Tanaka, J., and Mann, S. (2003). Dextran templating for the synthesis of metallic and metal oxide sponges. *Nat. Mat.* 2, 386–390. doi:10.1038/nmat903

Wang, H., Yang, B., Liao, X.-Z., Xu, J., Yang, D., He, Y.-S., et al. (2013). Electrochemical Properties of P2-$Na_{2/3}[Ni_{1/3}Mn_{2/3}]O_2$ cathode material for sodium ion batteries when cycled in different voltage ranges. *Electrochim. Acta* 113, 200–204. doi:10.1016/j.electacta.2013.09.098

Wang, K., Yan, P., and Sui, M. (2018). Phase transition induced cracking plaguing layered cathode for sodium-ion battery. *Nano Energy* 54, 148–155. doi:10.1016/j.nanoen.2018.09.073

Wang, P. F., Yao, H. R., Liu, X. Y., Yin, Y. X., Zhang, J. N., Wen, Y., et al. (2018). Na^+/vacancy disordering promises high-rate Na-ion batteries. *Sci. Adv.* 4, eaar6018–9. doi:10.1126/sciadv.aar6018

Wang, P., You, Y., Yin, Y., Wang, Y., Wan, L., Gu, L., et al. (2016). Suppressing the P2-O2 phase transition of $Na_{0.67}Mn_{0.67}Ni_{0.33}O_2$ by magnesium substitution for improved sodium-ion batteries. *Angew. Chem. Int. Ed.* 55, 7445–7449. doi:10.1002/anie.201602202

Wang, Y. B., Yang, Q., Guo, X., Yang, S., Chen, A., Liang, G. J., et al. (2022). Strategies of binder design for high-performance lithium-ion batteries: A mini review. *Rare Met.* 41, 745–761. doi:10.1007/s12598-021-01816-y

Wang, Y., Tang, K., Li, X., Yu, R., Zhang, X., Huang, Y., et al. (2019). Improved cycle and air stability of P3-$Na_{0.65}Mn_{0.75}Ni_{0.25}O_2$ electrode for sodium-ion batteries coated with metal phosphates. *Chem. Eng. J.* 372, 1066–1076. doi:10.1016/j.cej.2019.05.010

Wen, Y., Wang, B., Zeng, G., Nogita, K., Ye, D., and Wang, L. (2015). Electrochemical and structural study of layered P_2-type $Na_2/3Ni_1/3Mn_2/3O_2$ as cathode material for sodium-ion battery. *Chem. Asian J.* 10, 661–666. doi:10.1002/asia.201403134

Yabuuchi, N., Kubota, K., Dahbi, M., and Komaba, S. (2014). Research development on sodium-ion batteries. *Chem. Rev.* 114, 11636–11682. doi:10.1021/cr500192f

Zhang, J., Wang, W., Wang, W., Wang, S., and Li, B. (2019). Comprehensive review of P2-type $Na_{2/3}Ni_{1/3}Mn_{2/3}O_2$, a potential cathode for practical application of Na-ion batteries. *ACS Appl. Mat. Interfaces* 11, 22051–22066. doi:10.1021/acsami.9b03937

Zhang, L. (2019). *Electrochemical performance and structural changes of $Na_{0.67}Mn_{0.67}Ni_{0.33}O_2$ as cathode for sodium ion batteries (PhD thesis)*. Berlin: Technische Universität Berlin.

Zhang, L., Wang, J., Li, J. J., Schuck, G., Winter, M., Schumacher, G., et al. (2020a). Preferential occupation of Na in P3-type layered cathode material for sodium ion batteries. *Nano Energy* 70, 104535. doi:10.1016/j.nanoen.2020.104535

Zhang, L., Wang, J., Schuck, G., Xi, F., Du, L., Winter, M., et al. (2020b). Stabilizing P3-type oxides as cathodes for high-rate and long-life sodium ion batteries by disordered distribution of transition metals. *Small Methods* 4, 2000422. doi:10.1002/smtd.202000422

Zhang, X., Zhu, Y., Bruck, A. M., Housel, L. M., Wang, L., Quilty, C. D., et al. (2019). Understanding aggregation hindered Li-ion transport in transition metal oxide at mesoscale. *Energy Storage Mater.* 19, 439–445. doi:10.1016/j.ensm.2019.03.017

Zhang, Y.-Y., Zhang, S.-J., Li, J.-T., Wang, K., Zhang, Y.-C., Liu, Q., et al. (2019). Improvement of electrochemical properties of P2-type $Na_{2/3}Mn_{2/3}Ni_{1/3}O_2$ sodium ion battery cathode material by water-soluble binders. *Electrochim. Acta* 298, 496–504. doi:10.1016/j.electacta.2018.12.089

Zhang, Y., Wu, M., Ma, J., Wei, G., Ling, Y., Zhang, R., et al. (2020a). Revisiting the $Na_{2/3}Ni_{1/3}Mn_{2/3}O_2$ cathode: Oxygen redox chemistry and oxygen release suppression. *ACS Cent. Sci.* 6, 232–240. doi:10.1021/acscentsci.9b01166

Zhang, Y., Wu, M., Teng, W., Ma, J., Zhang, R., and Huang, Y. (2020b). Water-stable cathode for high rate Na-ion batteries. *ACS Appl. Mat. Interfaces* 12, 15220–15227. doi:10.1021/acsami.0c00386

Zhang, Y., Zhang, R., and Huang, Y. (2019). Air-stable $NaxTMO_2$ cathodes for sodium storage. *Front. Chem.* 7, 335. doi:10.3389/FCHEM.2019.00335

Zhao, Y. M., Yue, F. S., Li, S. C., Zhang, Y., Tian, Z. R., Xu, Q., et al. (2021). Advances of polymer binders for silicon-based anodes in high energy density lithium-ion batteries. *InfoMat* 3, 460–501. doi:10.1002/INF2.12185

Zheng, L., Li, J., and Obrovac, M. N. (2017). Crystal structures and electrochemical performance of air-stable $Na_{2/3}Ni_{1/3-x}Cu_xMn_{2/3}O_2$ in sodium cells. *Chem. Mat.* 29, 1623–1631. doi:10.1021/acs.chemmater.6b04769

Zheng, X., Li, P., Zhu, H., Rui, K., Zhao, G., Shu, J., et al. (2018). New insights into understanding the exceptional electrochemical performance of P2-type manganese-based layered oxide cathode for sodium ion batteries. *Energy Storage Mat.* 15, 257–265. doi:10.1016/j.ensm.2018.05.001

Zhou, Y. N., Wang, P. F., Zhang, X. D., Huang, L. B., Wang, W. P., Yin, Y. X., et al. (2019). Air-stable and high-voltage layered P3-type cathode for sodium-ion full battery. *ACS Appl. Mat. Interfaces* 11, 24184–24191. doi:10.1021/acsami.9b07299

Zilinskaite, S., Rennie, A. J. R., Boston, R., and Reeves-McLaren, N. (2018). Biotemplating: A sustainable synthetic methodology for Na-ion battery materials. *J. Mat. Chem. A* 6, 5346–5355. doi:10.1039/c7ta09260a

Zuo, W., Qiu, J., Liu, X., Ren, F., Liu, H., He, H., et al. (2020). The stability of P2-layered sodium transition metal oxides in ambient atmospheres. *Nat. Commun.* 11, 3544. doi:10.1038/s41467-020-17290-6